Silver-doped glass-ceramic scaffolds with antibacterial and bioactive properties for bone substitution

Ceramics International 50 (2024) 30997–31005

Contents lists available at ScienceDirect

Ceramics International

journal homepage: www.elsevier.com/locate/ceramint

Silver-doped glass-ceramic scaffolds with antibacterial and bioactive properties for bone substitution

Mari Lallukka, Marta Miola, Enrica Verné **, Francesco Baino *

Institute of Materials Physics and Engineering, Department of Applied Science and Technology (DISAT), Politecnico di Torino, Corso Duca Degli Abruzzi 24, 10129, Torino, Italy

ARTICLE INFO

Handling Editor: Dr P. Vincenzini

Keywords:
Bioactive glass
Glass-ceramic
Scaffold
Antibacterial

ABSTRACT

The preparation of scaffolds that are both macroporous and mechanically strong is a significant challenge in the development of bioactive ceramic materials for bone substitution. Furthermore, the introduction of beneficial extra-functionalities such as bacterial inhibition is highly appealing but adds complexity to implant design and production. In this study, we aimed to fabricate highly porous, bioactive and antibacterial glass-ceramic scaffolds with interconnected macropores through the foam replica method. The scaffolds were sintered at two different temperatures (620 and 850 °C), yielding glassy or partially crystallized materials, respectively. The scaffold produced at higher temperature was found to be highly porous (>75 vol%), mechanically stronger and able to induce hydroxyapatite formation after three days of soaking in SBF (*in vitro* bioactivity). In order to confer antibacterial activity, silver (Ag) ions were introduced onto the scaffold surface through ion exchange in an aqueous solution. Compositional analysis confirmed the successful doping of the scaffold surface with silver, which was continuously released in SBF for at least 28 days, as revealed by ICP-MS. Finally, the antibacterial action of the Ag-doped scaffold was confirmed towards *Staphylococcus epidermidis*. Overall, the results reported in this work show the potential of foam-like Ag-doped bioactive glass-ceramic scaffolds to be used in applications requiring bone substitution and antibacterial properties.

1. Introduction

The foam replica method refers to reproducing the porous structure of a sacrificial template to obtain its replicas from ceramic or glass particles, which are then sintered around the organic sacrificial template that is simultaneously burnt-off [1]. This method was first applied in 2006 by Chen et al. [2] and Park et al. [3] in the field of bone tissue engineering with a slurry containing bioactive glass particles, but the process concept was developed as early as the 1960s for other industrial applications, e.g. making filtering products [4]. Briefly, the method encompasses four main steps, i.e. template immersion in the glass (ceramic) particle-containing slurry, drying, burning out of the foam, and sintering of the material, which, like the choice of template, can be tuned to achieve the desired structural properties of the final product [1].

The advantages of the foam replica method include its simplicity, affordability, and effectiveness in developing highly porous and interconnected three-dimensional scaffolds [1]. For example, synthetic (e.g., polyurethane (PU) sponge [2,3]) or natural templates (e.g., marine sponges [5], demineralized bone matrix [6]) with different pore sizes and distributions can be selected for the foam replica method, and there is also the possibility of using either melt-derived [2,3] or sol-gel glasses [7,8] as well as glass-ceramics [9,10] in the slurry, which also makes the method very versatile.

Silver (Ag) could be incorporated into bioceramic-based scaffolds to add antibacterial properties using various processes such as coating, doping, and mixing in different forms [11], such as particles [12,13] and oxides [14–16]. Silver was incorporated for the first time into a porous bioactive glass scaffold in 2006 by the sol-gel foaming method [17]. Other examples of Ag-doped sol-gel glass-ceramic scaffolds by foam replica (PU sponge) are also reported in Refs. [15,18]. However, the sol-gel foaming process is complex and time-consuming, and porous products obtained from it are typically weak from a mechanical viewpoint. On the other hand, scaffolds prepared from melt-derived bioactive glass-ceramic powder have been Ag-doped by including $AgNO_3$ in the slurry [19]. Scaffolds prepared by the foam replica method can exhibit a

* Correspondence author.
** Corresponding author.
E-mail addresses: enrica.verne@polito.it (E. Verné), francesco.baino@polito.it (F. Baino).

https://doi.org/10.1016/j.ceramint.2024.05.404
Received 20 December 2023; Received in revised form 24 May 2024; Accepted 25 May 2024
Available online 28 May 2024

multiscale porosity if they combine melt-derived and sol-gel mesoporous bioactive glasses (MBGs). For instance, Ag-doped MBG-coated 45S5 melt-derived scaffolds were fabricated by using a natural marine sponge as a template [20]. Silver can also be added by a post-processing treatment: in this regard, 45S5 glass powder was used with PU foam to prepare scaffolds, which were then coated with Ag nanoparticles by immersing the scaffolds into the nanoparticle suspension [13].

In order to incorporate antibacterial silver only on the surface of the scaffold without affecting the material bulk properties, an ion exchange method has been implemented. In the process, the surface of the glass replaces its monovalent ions with the desired ions present in the ion exchange solution. For instance, the authors have developed Ag-doping processes in an aqueous solution of $AgNO_3$ for glass-ceramic scaffolds based on different glass composition and ion-exchange parameters [21] than the here-studied SBA2. In addition to using aqueous solution, Newby et al. have implemented a molten $AgNO_3$ salt bath to coat 45S5 foam-replicated scaffolds with Ag ions by ion exchange [22].

This study aimed to prepare 3D macroporous bioactive glass-ceramic foams, which were then characterized in terms of thermal, morphological, and mechanical properties. In addition, the possibility to dope the scaffold surface with antibacterial Ag ions via ion-exchange process in aqueous solution has been investigated. The effects of Ag-doping on the scaffold structure, composition and *in vitro* bioactivity have been assessed, along with the analysis of Ag-leaching in Simulated Body Fluid (SBF). Finally, the antibacterial effect of Ag-doped scaffold was investigated towards *Staphylococcus epidermidis*.

2. Materials and methods

2.1. Starting glass synthesis

A melt-derived silicate bioactive glass, referred to as SBA2 ($48SiO_2$–$18Na_2O$–$30CaO$–$3P_2O_5$-$0.43B_2O_3$-$0.57Al_2O_3$, in mol.%) was used as a starting material for scaffold fabrication. The SBA2 glass was synthesized by melting high-purity raw precursors (SiO_2, Na_2CO_3, $CaCO_3$, $Ca_3(PO_4)_2$, H_3BO_3, Al_2O_3, Sigma Aldrich) in a platinum crucible in the air at 1450 °C for 1 h. The melt was then quenched into distilled water to obtain a frit, which was dried at room temperature and further ground by zirconia ball milling (Pulverisette 0, Fritsch, Germany). The obtained glass powder was sieved by using a stainless-steel sieve (Giuliani Technologies Srl, Italy) to obtain particles with size below 32 μm for scaffold fabrication.

2.2. Glass characterization by thermal analyses

The glass transition temperature (T_g), onset of crystallization temperature (T_x) and peak crystallization temperature (T_c) of the SBA2 glass were determined by differential thermal analysis (DTA; DTA404PC, Netzsch, Germany). The heating rate used was 5 °C/min 50 mg of SBA2 powder was heated to 1300 °C in a platinum crucible using Al_2O_3 powder as a reference. The characteristic temperatures were determined from the DTA plot (T_g at the inflection point, T_x at the onset point of the exothermic peak from the first derivative of the thermogram, T_c at the maximum of the exothermic peak).

Hot stage microscopy (HSM; Hesse Instruments EM 301, Hesse Instruments, Germany) was performed to quantify the shrinkage due to sintering by measuring the variation of specimen size during a controlled heating process. HSM was performed in the air, and the heating rate used was 5 °C/min. The pellet of SBA2 was prepared by manually pressing SBA2 powder using a small cylindrical mold.

2.3. Scaffold fabrication

The scaffolds were fabricated by following a modified version of the protocol described elsewhere [23]. Shortly, a commercially available PU foam in the form of cubic blocks (10 × 10 × 10 mm^3) was used as the scaffold template. The cubes were immersed in a water-based slurry with a weight composition of 30 % SBA2 glass, 64 % distilled water, and 6 % of poly(vinyl alcohol) (PVA) used as a binder. Briefly, the PVA granules were dissolved in water under continuous stirring at 80 °C. The water evaporated during PVA dissolution was added back to the slurry to achieve the desired weight composition. Then, the SBA2 powder was dispersed in the solution and stirred until a homogeneous mixture was obtained. The PU foam cubes were immersed into the slurry for 60 s, extracted, and compressed along the three spatial directions to 60 % of thickness to uniformly remove the excess slurry. The impregnation/compression cycle was repeated three times and, finally, the fourth cycle was repeated without compression. The cubes were dried at room temperature for 6 h and thermally treated to remove the organic template and sinter the inorganic phase. The SBA2-derived scaffolds were sintered for 3 h at 620 °C to obtain an amorphous material (SBA2-620), or at 850 °C to produce a glass-ceramic (SBA2-850).

The Ag-doping of the outermost surface layer of the scaffold was performed by ion exchange only for the scaffolds sintered at 850 °C (SBA2-850), being the most promising according to the results from mechanical tests. The ion exchange was performed by following the original protocol optimized for bulk glass discs [24,25]. Briefly, the porous SBA2-derived cubes were immersed in an aqueous solution of 0.03 M $AgNO_3$ (Sigma Aldrich) and soaked at 37 °C for 1 h. Then, the cubes were rinsed with bi-distilled water and left to dry in ambient conditions. The Ag-doped glass-derived scaffolds will be referred to as Ag-SBA2 from now on.

2.4. Scaffold characterization

2.4.1. Scaffold morphology, porosity, and crystalline structure

The morphology and architecture of the scaffolds were studied using both Scanning Electron Microscopy (SEM, JCM-6000Plus, JEOL) and Field Emission Scanning Electron Microscopy, (FESEM, Merlin electron microscope, ZEISS, Germany). A thin layer of platinum was used as a coating on scaffolds to make them conductive prior to the analysis. FESEM equipped with Energy-dispersive X-ray Spectroscopy (EDS) was utilized for morphological and elemental analyses (maximum working voltage 15 kV).

The total porosity of scaffolds was estimated by density measurements. The density of the scaffolds was determined from the mass and volume of the sintered cubes. Then, the volumetric porosity (vol%) of the scaffolds was calculated by applying the following formula:

$$1 - \frac{\rho_s}{\rho_0} \times 100\% \quad (1)$$

where ρ_s is the density of sintered scaffold, and ρ_0 is the typical density of solid (non-porous) bioactive glass (2.7 g/cm^3) [26].

X-ray diffraction (XRD, Malvern PANalytical X'Pert PRO diffractometer), using the Bragg-Brentano camera geometry and the Cu Kα incident radiation, was performed on both types of scaffolds (SBA2-620 and SBA2-850) to study their crystalline structure and phase composition. The 2θ range used for sample measurements was from 10° to 70°. The data from the obtained XRD patterns were further analyzed by using the X-Pert HighScore Software and ICDD PDF database.

2.4.2. Mechanical properties

In order to evaluate the mechanical strength of the scaffolds, crushing tests (MTS Criterion Model 43, cross-head speed = 0.5 mm/min) were performed to obtain the stress-strain curves and, hence, the values of maximum compressive strength. Samples with parallel surfaces were used for these tests. The compressive strength was calculated as the ratio between the maximal load registered during the test (peak load) and the cross-sectional resistant area.

Similar crushing tests were also performed for Ag-doped scaffolds to compare the mechanical properties of undoped and Ag-doped scaffolds.

2.4.3. In vitro bioactivity and ion leaching test

The *in vitro* bioactivity of scaffolds was evaluated by immersing the samples in Simulated Body Fluid (SBF) according to the protocol developed by Kokubo and Takadama [27]. The mass-to-volume ratio between the scaffolds and SBF was 1.5 mg/mL, according to the recommendation of the TC04 glass Committee [28]. The SBF-immersed cubes were kept in an orbital shaker (37 °C, 120 RPM) for 1 day, 3 days, 7 days, 14 days, and 28 days. The pH of the solutions was monitored at every timepoint.

In order to investigate the apatite-forming ability of scaffolds, the SBF-soaked cubes were then analyzed by FESEM-EDS. Prior to the FESEM-EDS analysis, the scaffolds were coated with a thin layer of chromium. In addition, Fourier-transform infrared spectroscopy with an attenuated total reflectance (ATR) equipment (FTIR-ATR, Nicolet, iS50 FTIR Spectrometers, Thermo Scientific), using software OMNIC, was utilized to identify the formation of reaction phases during the immersion of the scaffolds in SBF. The FTIR measurement was performed on the powder of the newly-formed phase (white particles) that could be easily removed by using a spatula from the surface of the SBF-immersed scaffolds; the frequency range of 400–4000 cm^{-1} was considered, accumulating 16 scans with a resolution of 4 cm^{-1}.

In addition, Ag leaching in SBF was quantified by Inductively coupled plasma mass spectrometry (ICP-MS; iCAP Q ICP-MS, Thermo Fischer Scientific).

2.4.4. Antibacterial properties

The preliminary evaluation of the antibacterial potential was performed by the inhibition zone test (Kirby-Bauer test) according to the NCCLS protocol [29], using a standard strain of *Staphylococcus epidermidis* (ATCC 12228). The reason for choosing *S. epidermidis* is its common involvement in bone infections [30]. Briefly, a 0.5 McFarland solution, which contains approximately 1×10^8 colony forming units (CFU)/mL, was prepared by introducing some *S. epidermidis* colonies, grown on a blood agar plate, in physiological solution; the turbidity of the solution was determined with an optical instrument—Phoenix Spec BD McFarland (Becton, Dickinson and Company, Franklin Lakes, NJ, USA). This bacterial suspension was evenly distributed on a Mueller Hinton agar plate (Becton, Dickinson and Company, Franklin Lakes, NJ, USA), and the scaffolds were placed in contact with the agar and incubated overnight at 37 °C. At the end of incubation, the inhibition zone was observed and measured.

2.5. Statistical analysis

Results of porosity calculation, mechanical tests, and antibacterial experiments were expressed as mean ± standard deviation. Statistical differences between the groups were analyzed by Student's t-test ($p < 0.05$) and properly indicated, if relevant.

3. Results and discussion

In order to decide the sintering temperatures for scaffolds, DTA and HSM analyses were performed on the cylindrical pellets compacted from the SBA2 glass powder. Combined DTA and HSM graphs are shown in Fig. 1.

As shown in Fig. 1, the glass transition temperature was detected around 570 °C.

The HSM curve (Fig. 1B) reveals that SBA2 exhibits a one-step densification behavior (ΔS_{TOT} around 30 %). The glass starts to shrink around the glass transition temperature detected by the DTA analysis. This is also the very beginning of viscous flow sintering. The pellet continues to shrink and reaches the maximum shrinkage at Tx (around 670 °C). If the temperature keeps increasing, glass expansion is detected, which is seen as increasing A_T/A_0. Around the melting onset at 1150 °C the glass is seen shrinking rapidly again in the HSM curve. Similar expansion is seen in other papers dealing with bioactive glasses [31] or non-biomedical glass compositions [32].

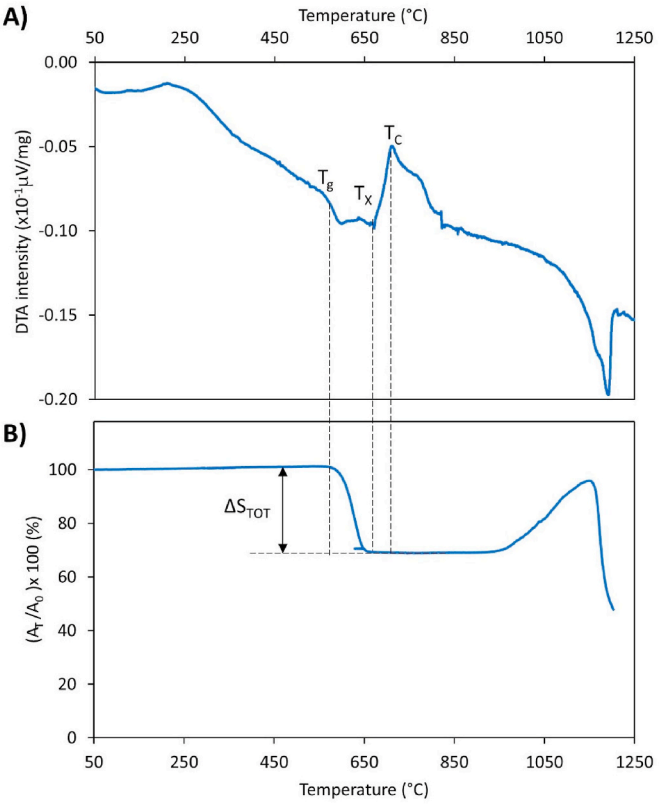

Fig. 1. Thermal analyses on SBA2: A) DTA plot with Tg = glass transition temperature, Tx = onset crystallization temperature, and Tc = peak crystallization temperature; and B) HSM plot, shrinkage variation as a function of temperature, ΔS_{TOT} = maximum shrinkage.

From the viewpoint of glass stability against crystallization, the difference between Tx and Tg ($T_X - T_g$ = 670–570 = 100 °C) can be examined. In general, the greater this difference, the lower the tendency for the glass to crystallize upon heating.

Another way to assess the glass stability relies on assessing the Hruby parameter K_H [33]:

$$K_H = \frac{T_X - T_g}{T_M - T_x} \quad (2)$$

As a rule of thumb, the greater the K_H, also the greater the glass stability against crystallization upon heating. In the case of SBA2 glass, we found $K_H = 0.192$, which is higher – for example – than the Hruby parameter assessed for 45S5 glass, in which sintering and crystallization are competing phenomena [31].

Sinterability can also be quantified by using the parameter $S_C = T_X - T_{MS}$, where T_{MS} is the temperature of maximum shrinkage detected by HSM measurement [32]. In our case S_C = 670–650 = 20 °C > 0, which would suggest full sintering before crystallization [32]; in other words, we could theoretically obtain a totally amorphous product after sintering. On the other hand, achieving adequate densification – and hence satisfactory mechanical properties – may require long time if sintering is performed below Tx.

Therefore, based on the thermal analyses, the glass SBA2 seems to exhibit a high sinterability and is suitable for being used for scaffold fabrication. However, because the DTA and HSM analyses were performed on cylindrical pellets compacted from the glass powder instead of scaffold cubes with polymeric PU foam inside, these results are only a starting point to find optimal sintering temperature.

Based on thermal analyses, two different sintering temperatures, T_{s1} and T_{s2}, were chosen for further characterization:

1) $T_{s1} = T_g + 50$ °C, to obtain an amorphous glass scaffold (sintering at 620 °C), and
2) T_{s2} well after the detected T_C, to obtain a glass-ceramic scaffold with full densification and expected higher mechanical strength (sintering at 850 °C).

Next, the morphology and architecture of sintered scaffolds were evaluated by SEM (Fig. 2).

As shown in Fig. 2, PU sponge architecture was faithfully replicated for both scaffolds, thus successfully mimicking the structure of natural cancellous bone. Smoother and more densified struts as well as less distinguishable single glass particles were seen in the scaffold sintered at higher temperature (Fig. 2B and D, 850 °C). Also at the macroscale, the cubes are seen to maintain their shape, although the shrinkage of the cubes is evident due to sintering.

Next, both scaffolds were characterized by XRD analysis to investigate any formation of crystalline phases (Fig. 3).

The XRD pattern of SBA2 glass without any heat treatment is reported elsewhere [25]. As regards SBA2-620 (Fig. 3), a broad halo was detected along with some very minor diffraction peaks due to the initial nucleation of combeite ($Na_2Ca_2Si_3O_9$, ref 00-002-0961); however, the XRD pattern reveals a predominantly amorphous material. The SBA2-850 scaffold was found to be glass-ceramic with many evident crystalline peaks. The two main phases identified were combeite ($Na_2Ca_2Si_3O_9$, ref 00-002-0961), and silicorhenanite ($Na_2Ca_4(PO_4)_2SiO_4$, ref 00-032-1053). Similar peaks have been reported by other authors regarding thermally treated 45S5 glass [2,34,35], thus suggesting the high biocompatibility of SBA2-derived materials.

In general, the mechanical properties of a 3D scaffold can be determined by using stress-strain curves and the maximum compressive strength can be derived from these plots. Fig. 4 displays some examples of the typical stress-strain curves of the scaffolds produced.

For all scaffolds, multiple peaks ("jagging") are detected on the stress-strain curve. The reason for that is typical of brittle porous ceramics: when a load is applied to the scaffold, the thinnest struts break at stress-concentrating sites, which causes a temporary decline of the stress [31]. On the other hand, the overall structure can still bear increasing loads, thus determining the new increase in stress values. First, a positive slope is noted until the maximum temporary stress is reached. Then, thicker struts of the scaffold start to fracture, which leads to a negative slope. The repetition of this behaviour yields the irregular profile of the stress-strain curve [2].

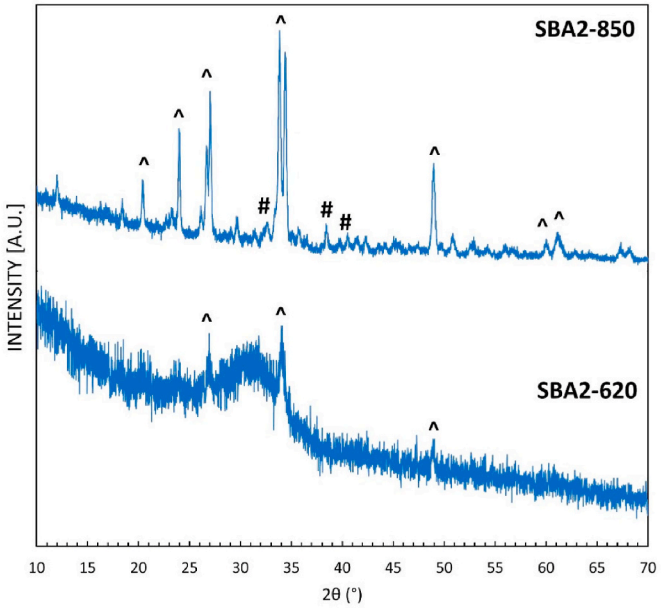

Fig. 3. XRD patterns of SBA2 scaffolds sintered at 620 °C and 850 °C. ^ = combeite, # = silicorhenanite.

Table 1 summarizes the porosity and compressive strength values of all scaffold types.

As reported in Table 1 and Fig. 4, the glass-ceramic scaffolds possess superior compressive strength compared to the amorphous ones. This phenomenon was expected as it is generally known that the crystalline phases embedded in the amorphous matrix can enhance the strength and fracture toughness of the glass [36]. Indeed, also higher sintering temperature will lead to more densified and stronger struts of the scaffold,

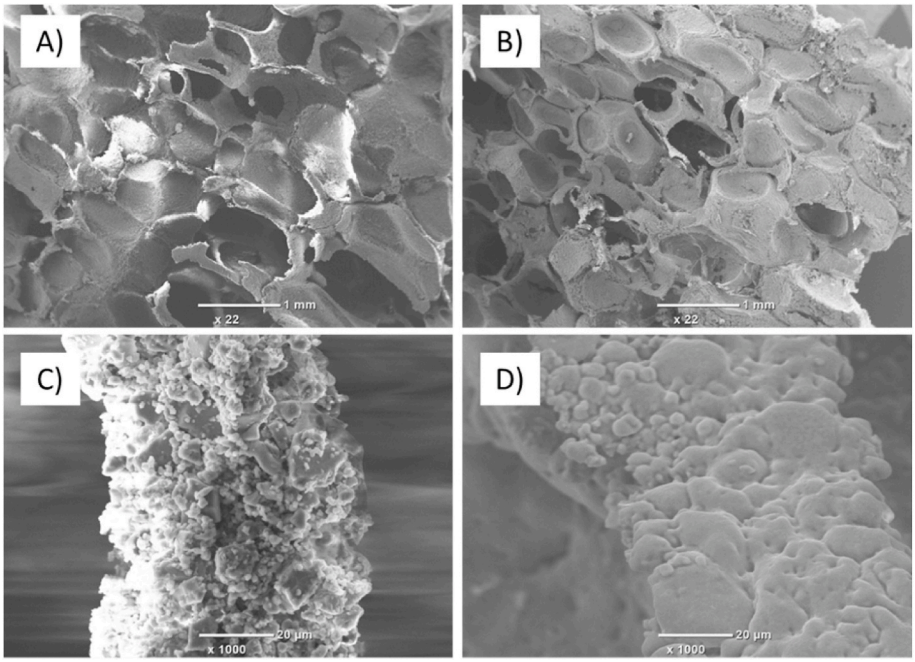

Fig. 2. Architecture and morphology of SBA2-derived scaffolds: A) SBA2-620 scaffold (magn. 22×); B) SBA2-850 scaffold (magn. 22×); C) SBA2-620 scaffold (magn. 1000×); D) SBA2-850 scaffold (magn. 1000×).

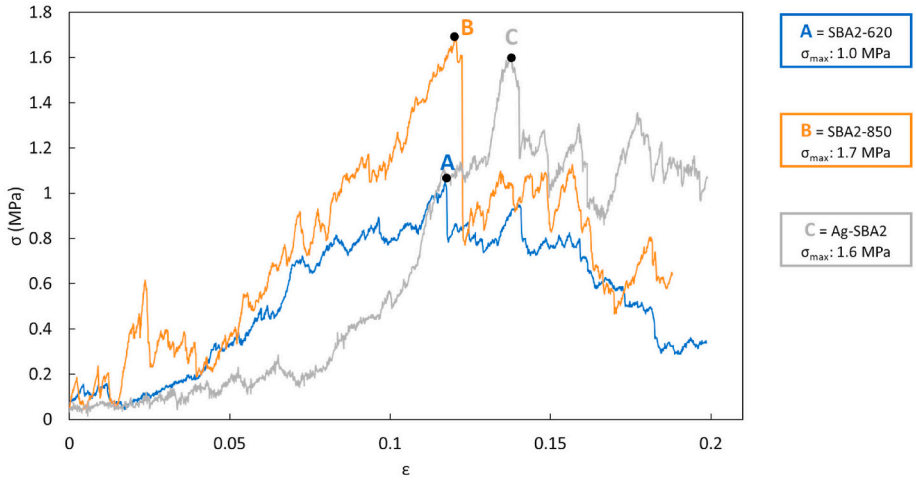

Fig. 4. Examples of stress-strain curves of SBA2-derived scaffolds sintered at 620 °C and 850 °C, and Ag-doped scaffold sintered at 850 °C. The peak stress points are indicated with A, B, and C.

Table 1
Comparison of the scaffold features.

Scaffold	Total porosity (vol%)	Peak stress (compression) (MPa)
SBA2-620	74.6 ± 2.8	0.9 ± 0.2
SBA2-850	75.1 ± 1.4	1.5 ± 0.3
Ag-SBA2 (850 °C)	77.4 ± 4.9	1.4 ± 0.3

hence achieving greater compressive strength.

The compressive strength of glass-ceramic scaffold was found comparable to that of cancellous bone. The compressive strength of spongy bone (not the single strut) is around 0.2–4 MPa [2]. Since the scaffolds are intended for use in contact with bone tissue, it is important to match the mechanical properties with the ones of hard tissue. A lower mechanical strength can lead to failure of the material and, on the other hand, a strength higher than that of the bone can lead to stress shielding phenomenon.

The compressive strength is directly related to the porosity level and the organization of the struts in the 3D space. As seen in Table 1, SBA2-620 and SBA2-850 scaffolds have a high degree of porosity (~75 vol%) with no statistically significant difference. In general, highly interconnected porosity of a scaffold is essential to promote bone and vascular ingrowth [37]. However, the strength and stiffness progressively decrease when the volume fraction of porosity increases and, therefore, it is important to balance porosity and mechanical integrity. Other factors affecting the mechanical properties include the composition of the initial glass and the slurry, and parameters of the foam replica method, such as the number of consecutive dipping cycles and the duration of every single immersion. Indeed, also the sintering temperature and heating rate used play an important role in the process.

Due to the unsatisfactory mechanical properties of the amorphous scaffold, further experiments and characterization are performed only for the glass-ceramic scaffolds (i.e., SBA2-850). By using ion exchange in aqueous solution of silver nitrate, the glass-ceramic scaffolds were doped with Ag-ions (Ag-SBA2) on their surface to add antibacterial properties.

The morphology and compositional analyses (by EDS) of Ag-doped scaffold are shown in Fig. 5.

Compositional analysis confirmed the incorporation of Ag on the scaffold surface, as revealed by EDS spectrum. FESEM analysis on

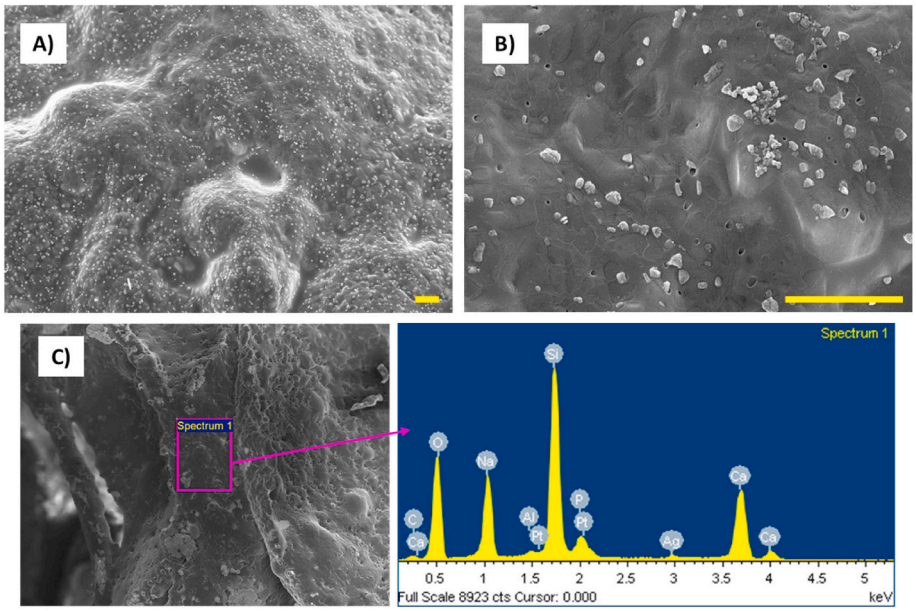

Fig. 5. A) and B) FESEM of Ag-SBA2 scaffold, scale bars 1 μm. C) EDS analysis of the Ag-SBA2 scaffold surface.

scaffold struts also revealed the presence of small particles with size around 100–200 nm, which can be attributable to a silver-containing phase. This finding is consistent with the results reported in a previous work, where silver carbonate particles were found on the surface of the same glass after the ion-exchange process in silver nitrate [25]. However, quantification is not possible due to the very small amount of silver (which is close to the detection limit for this technique) and the curvature of the surface analyzed.

Next, the mechanical crushing test was performed on Ag-SBA2 scaffolds to see whether the ion-doping on the scaffold surface might affect the compressive strength (Fig. 4). As displayed in Fig. 4 and Table 1, no statistically significant difference was found between undoped and Ag-doped scaffolds in terms of total porosity and maximum compressive strength. Therefore, the process of Ag-doping does not seem to affect the mechanical strength of the scaffolds.

The characterization of Ag-SBA2 scaffold was continued by analyzing the *in vitro* bioactivity through immersing the samples in SBF up to 28 days. The results of the test (FESEM images, EDS analysis) are reported in Fig. 6 and Table 2.

As shown in Fig. 6, for both undoped and Ag-doped scaffolds the typical globular "cauliflower" morphology of hydroxyapatite is visible already after 3 days of immersion in SBF. After 14 days, the struts of scaffolds are continuously coated with hydroxyapatite. The compositional analysis by EDS (Table 2) further confirms the fast bioactivity kinetics because the calculated Ca/P ratio suggests the surface to be coated with a hydroxyapatite-like layer. The Ca/P stoichiometric ratio of natural hydroxyapatite is known to be 1.67 [38], which is very close to the value registered here, already after one day of soaking in SBF. These results are in line with theoretical expectations: although aluminium oxide is known to reduce glass dissolution and, hence, bioactivity, the small amount of Al_2O_3 contained in SBA2 composition has negligible effects on these properties (a comprehensive study by Andersson et al. reported the suppression of bioactivity in silicate/borosilicate glass systems only if the Al_2O_3 content is above 1.5 wt% [39].

Table 2
Ca/P ratio of SBF-soaked Ag-SBA2 and SBA2-850 scaffolds derived from the EDS analysis.

Ca/P atomic ratio	Time point (day)				
	0d	*1d*	*3d*	*7d*	*14d*
SBA2-850	5.68	1.89	1.89	2.32	1.58
Ag-SBA2	5.28	1.79	1.88	1.75	1.89

In general, the glass-ceramic nature of the scaffold seems not to suppress the bioactivity mechanism. In previous works, amorphous SBA2 glass discs have been found to show some hydroxyapatite precipitation already after one day of soaking in SBF, and a clear layer of hydroxyapatite was observed after 3 days in SBF [40]. In a porous scaffold, the reactive surface is larger as compared to bulk samples, which can indeed accelerate the bioactivity kinetics. This is seen also in our case with fast hydroxyapatite nucleation and a fast increase in the pH of the soaking solution during the immersion.

The bioactivity of the glass-ceramic scaffolds was further investigated by FTIR analysis. Fig. 7 displays the FTIR-ATR spectra of both undoped and Ag-doped scaffolds prior (0d) and after [1-28d] SBF immersion.

When comparing the FTIR spectra of 1-28d soaked scaffolds to the 0d unsoaked one, there are clear differences in terms of peak intensities. However, spectra of undoped and Ag-doped scaffolds exhibit similar characteristic bands without any significant differences regarding to their peak positions.

For the 0d control samples, the main band corresponds to the V_{asym} (Si–O–Si) intense broad band at 1020 cm^{-1}, with an overlapping to phosphate group as both PO and SiO groups absorb in this region.

For 1-day soaked scaffolds, a band around 560-610 cm^{-1} can be detected, which is characteristic for amorphous calcium phosphate formation [41,42]. In addition, the presence of a broad band at ~1450 cm^{-1} corresponds to $\nu_3(CO_3^{2-})$ band of carbonates adsorbed on the

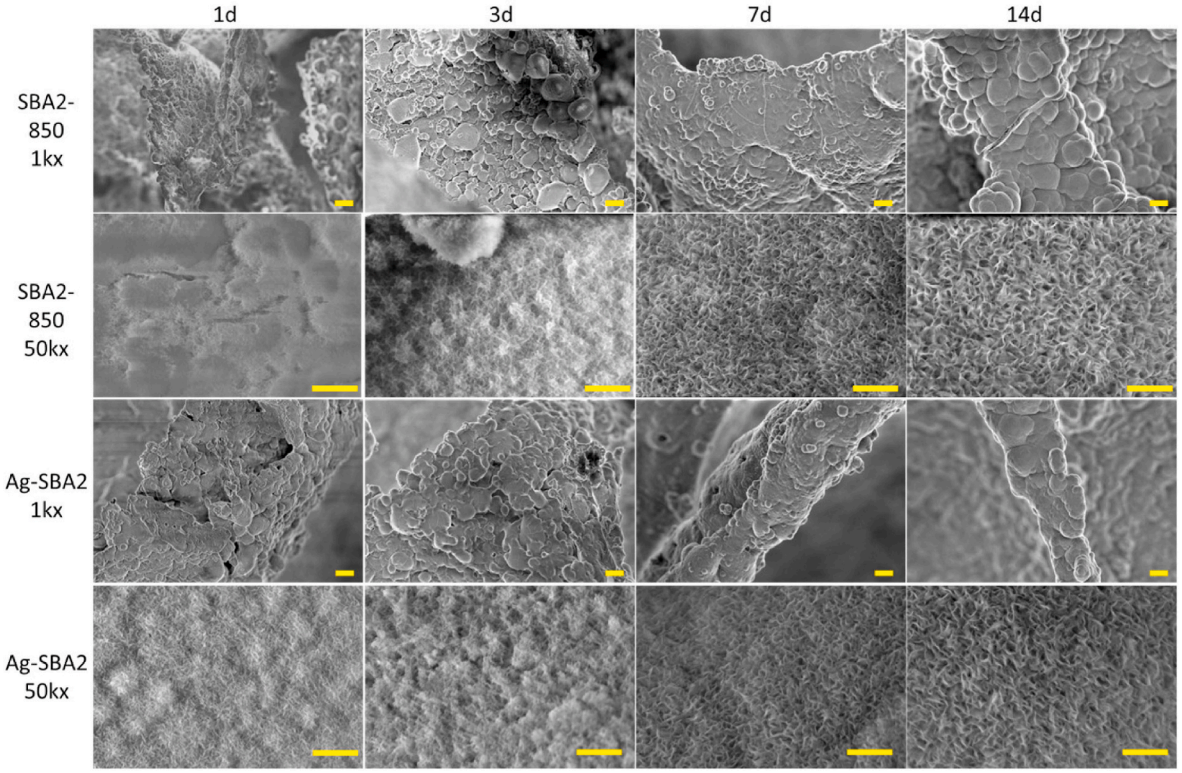

Fig. 6. FESEM images of the morphology of SBF-soaked SBA2-850 scaffolds, undoped and doped with Ag, up to 14 days. Scale bars: 20 μm for 1000× magnification, 1 μm for 50kx magnification.

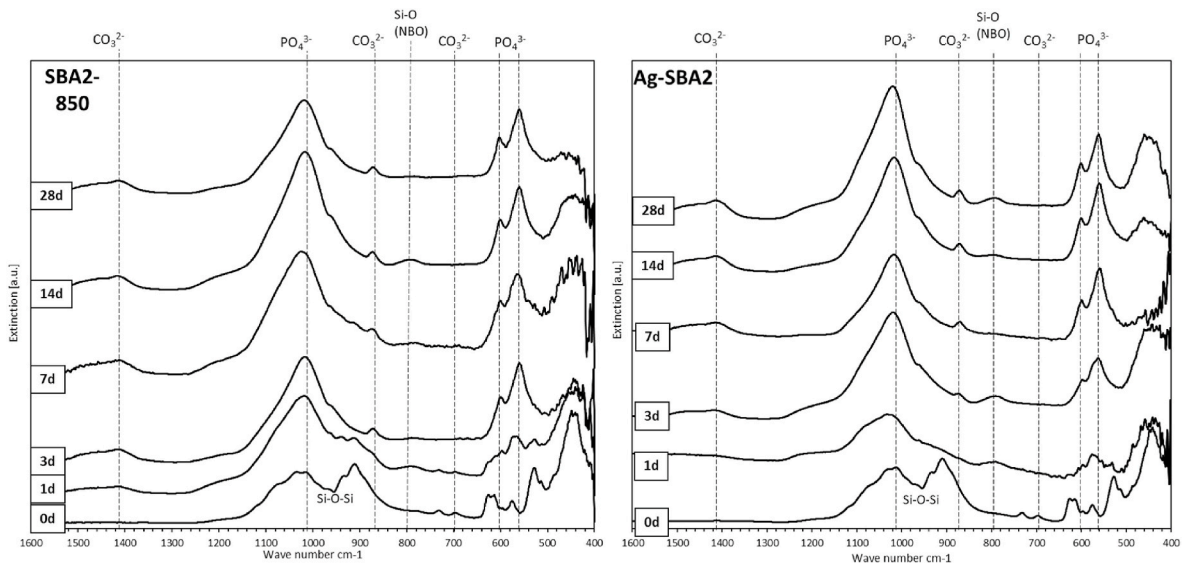

Fig. 7. FTIR-ATR spectra of SBF-soaked scaffolds up to 28 days. 0d is the control without SBF immersion. On the left: undoped SBA2-850, and on the right: Ag-SBA2 scaffold.

surface [42,43], which suggests B-type substitution, e.g., a carbonate replacing a phosphate group [44]. This peak also gets more evident after 3 days of soaking in SBF.

A sharpened phosphate band at ~1015 cm^{-1} [44] is already visible in scaffolds immersed for 1 day. The peak intensity increases, and the peak sharpens starting from 3 days of SBF immersion.

From 3 days of SBF soaking, at ~570 and ~600 cm^{-1} a sharp double band is detected. This indicates the presence of V_4(P–O–P), the bending mode of P–O–P bond in hydroxyapatite, or possibly other calcium orthophosphates, including octacalcium phosphate [42,44]. This is in line with our observations from FESEM and EDS (Fig. 6 and Table 2), where hydroxyapatite can be detected after 3 days of immersion for both SBA2-850 and Ag-SBA2 scaffolds.

Another characteristic band seen after 3 days of soaking is $V_2(CO_3^{2})$ sharp peak at ~871 cm^{-1}, corresponding to CO_3^{2-} group, which indicates carbonate substitution in the apatite, resulting in hydroxycarbonate apatite [44,45].

In addition to studying the bioactivity kinetics of the glass-ceramic scaffolds, the leaching of Ag during SBF soaking was also evaluated by ICP-MS (Fig. 8).

As displayed in Fig. 8, more than half of the total of Ag (around 450 ppb) was released during the first 24 h. Similar release profiles of rapid initial release of Ag ions from bioactive glass scaffolds have also been observed in the literature [46]. In general, this type of fast initial release of antibacterial agents is the most beneficial to prevent early infection after surgical treatment. However, Ag release continues up to 28 days without any noticeable plateau suggesting that some amount of silver remains on the surface of the scaffold. Although the first couple of days are the most critical for the development of post-surgical infections, it would also be useful to have prolonged release to maintain antibacterial effect in case of late infections [47].

Finally, an assessment of the antibacterial performance of the Ag-SBA2 scaffolds was performed by the inhibition zone test.

A clear color difference between white undoped and brownish Ag-SBA2 scaffolds can be detected, as shown in Fig. 9. The presence of silver oxide (Ag_2O) or carbonate, which can form during the ion exchange process, can cause brown coloration of the scaffold. The inhibition zone test towards *S. epidermidis* strain demonstrated the antibacterial effect of Ag-SBA2 scaffold. A clear inhibition zone of about 4–5 mm is detected around Ag-SBA2 scaffolds, while no halo is seen for the control (undoped) samples. Ag-SBA2 bulk discs have been previously shown to elicit antibacterial effects reducing surface colonization by drug-resistant strain of *Staphylococcus aureus* [48]. In addition, the antibacterial Ag-SBA2 discs were cytocompatible with both bone progenitor cells [48] and human adipose stem cells [49]. However, in order to verify and further characterize the antibacterial properties of porous 3D Ag-SBA2 scaffolds instead of bulk discs, more antibacterial tests

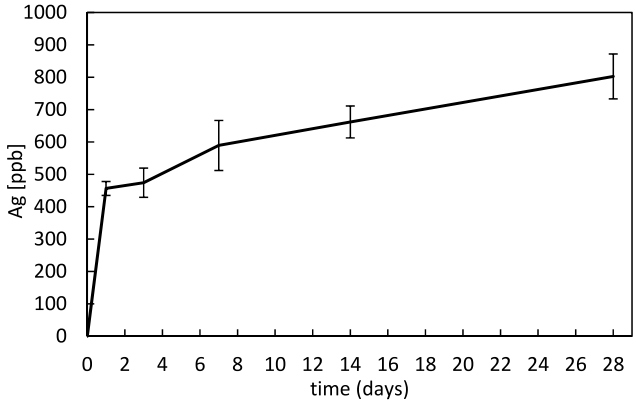

Fig. 8. Ag-leaching from Ag-SBA2 scaffolds soaked in SBF.

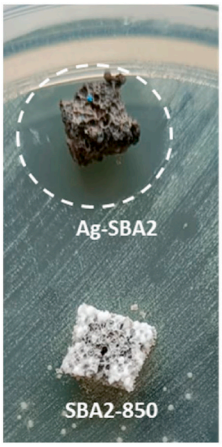

Scaffold	Halo size
SBA2-850	0.0 ± 0.0 mm
Ag-SBA2	4.3 ± 0.4 mm

Fig. 9. Antibacterial zone of inhibition against *S. epidermidis*.

(bacteria proliferation metabolic assay, CFU count) are planned for the future. Furthermore, it is critical to balance between antibacterial capability and biocompatibility and, therefore, cytocompatibility tests are also needed in the future.

4. Conclusions

In this work, porous bioactive glass-based scaffolds (parent SBA2 oxide system) using the foam replica method were successfully prepared and characterized. Two different sintering temperatures were compared: one resulting in an amorphous scaffold (620 °C), and another one yielding a glass-ceramic one (850 °C). Both scaffolds closely resembled the 3D architecture of natural trabecular bone and exhibited high porosity of approximately 75 vol%. However, due to its superior mechanical properties, only the glass-ceramic scaffold was the focus of further analyses.

The selected glass-ceramic scaffold SBA2-850 was then subjected to silver doping via ion exchange in aqueous solution, which did not alter either the 3D architecture or the mechanical strength of the glass-ceramic sample. Silver was found to be successfully introduced, covering the scaffold surface. When comparing the *in vitro* bioactivity of both Ag- and undoped SBA2-850 scaffold, no significant difference was observed. Both scaffolds were highly bioactive, promoting the precipitation of hydroxyapatite after just three days of soaking in SBF, as confirmed by FESEM, EDS and FTIR analysis. Furthermore, the antibacterial performance of the Ag-SBA2 scaffolds towards *S. epidermidis* was successfully demonstrated, and the Ag leaching behavior in SBF was found to be optimal for preventing both early and late infections after surgery.

Although the compressive strength of the obtained scaffold (around 1.5 MPa) was satisfactory and comparable to that of natural bone, alternative fabrication techniques, such as additive manufacturing, may yield even stronger scaffolds with higher mechanical performance and reproducibility. The foam replication was adopted in this study to initially validate the feasibility of the here proposed concepts, i.e. the study of a bone-like, bioactive and antibacterial multifunctional scaffold. Looking at the future, the scaffold developed in this study could find a possible application as a bone substitution material with antibacterial properties without using traditional antibiotics. This would be a significant achievement considering the current societal and medical challenges related to the abuse of antibiotics and bacterial resistance issues. However, further research deserves to be carried out to evaluate the biocompatibility of these scaffolds for potential clinical applications.

CRediT authorship contribution statement

Mari Lallukka: Data curation, Investigation, Methodology, Writing – original draft, Conceptualization. **Marta Miola:** Conceptualization, Investigation, Methodology, Supervision, Validation, Writing – review & editing. **Enrica Verné:** Conceptualization, Methodology, Project administration, Supervision, Validation, Writing – review & editing. **Francesco Baino:** Conceptualization, Investigation, Methodology, Supervision, Validation, Writing – review & editing.

Declaration of competing interest

The authors declare that they have no known competing financial interests or personal relationships that could have appeared to influence the work reported in this paper.

Acknowledgements

This study was funded by the European Union's Horizon 2020 Research and Innovation Program under Marie Skłodowska-Curie grant agreement No 860462-Project PREMUROSA.

References

[1] J. Chen, A. Roether, A. Boccaccini, Tissue engineering scaffolds from bioactive glass and composite materials, Top Tissue Eng 4 (2008 Jan 1).
[2] Q.Z. Chen, I.D. Thompson, A.R. Boccaccini, 45S5 Bioglass®-derived glass–ceramic scaffolds for bone tissue engineering, Biomaterials 27 (11) (2006 Apr 1) 2414–2425.
[3] Y.S. Park, K.N. Kim, K.M. Kim, S.H. Choi, C.K. Kim, R.Z. Legeros, et al., Feasibility of three-dimensional macroporous scaffold using calcium phosphate glass and polyurethane sponge, J. Mater. Sci. 41 (13) (2006 Jul 1) 4357–4364.
[4] S. Karl, A.V. Somers, Method of making porous ceramic articles [Internet]. US3090094A, Available from: https://patents.google.com/patent/US3090094A/en, 1963. (Accessed 3 February 2023).
[5] E. Cunningham, N. Dunne, Comparative characterisation of 3-D hydroxyapatite scaffolds developed via replication of synthetic polymer foams and natural marine sponges [Internet], J. Tissue Sci. Eng. (2011). s1. Available from: https://www.omicsonline.org/comparative-characterisation-of-3-d-hydroxyapatite-scaffolds-developed-via-replication-of-synthetic-polymer-foams-and-natural-marine-sponges-2157-7552.S1-001.php?aid=2213. (Accessed 3 February 2023).
[6] W. Xia, J. Chang, Bioactive glass scaffold with similar structure and mechanical properties of cancellous bone, J. Biomed. Mater. Res. B Appl. Biomater. 95B (2) (2010) 449–455.
[7] C. Navalón, P. Ros-Tárraga, A. Murciano, P. Velasquez, P. Mazón, P.N. De Aza, Easy manufacturing of 3D ceramic scaffolds by the foam replica technique combined with sol-gel or ceramic slurry, Ceram. Int. 45 (15) (2019 Oct 15) 18338–18346.
[8] S. Cabanas-Polo, A. Philippart, E. Boccardi, J. Hazur, A.R. Boccaccini, Facile production of porous bioactive glass scaffolds by the foam replica technique combined with sol–gel/electrophoretic deposition, Ceram. Int. 42 (5) (2016 Apr 1) 5772–5777.
[9] N.M. Possolli, F. Raupp-Pereira, O.R. Klegues Montedo, S. Arcaro, LZS bioactive glass-ceramic scaffolds: colloidal processing, foam replication technique and mechanical properties to bone tissue engineering, Open Ceram 9 (2022 Mar 1) 100219.
[10] E.A. Aguilar-Reyes, C.A. León-Patiño, E. Villicaña-Molina, V.I. Macías-Andrés, L. P. Lefebvre, Processing and in vitro bioactivity of high-strength 45S5 glass-ceramic scaffolds for bone regeneration, Ceram. Int. 43 (9) (2017 Jun 15) 6868–6875.
[11] C. Zhao, W. Liu, M. Zhu, C. Wu, Y. Zhu, Bioceramic-based scaffolds with antibacterial function for bone tissue engineering: a review, Bioact. Mater. 18 (2022 Dec 1) 383–398.
[12] C. Shuai, Y. Xu, P. Feng, G. Wang, S. Xiong, S. Peng, Antibacterial polymer scaffold based on mesoporous bioactive glass loaded with in situ grown silver, Chem. Eng. J. 374 (2019 Oct 15) 304–315.
[13] R.L.M.S. Oliveira, L. Barbosa, C.R. Hurtado, L. de P. Ramos, T.L.A. Montanheiro, L. D. Oliveira, et al., Bioglass-based scaffolds coated with silver nanoparticles: synthesis, processing and antimicrobial activity, J. Biomed. Mater. Res. 108 (12) (2020) 2447–2459.
[14] X. Chatzistavrou, J.C. Fenno, D. Faulk, S. Badylak, T. Kasuga, A.R. Boccaccini, et al., Fabrication and characterization of bioactive and antibacterial composites for dental applications, Acta Biomater. 10 (8) (2014 Aug 1) 3723–3732.
[15] A.C. Marsh, N.P. Mellott, M. Crimp, A. Wren, N. Hammer, X. Chatzistavrou, Ag-Doped bioactive glass-ceramic 3D scaffolds: microstructural, antibacterial, and biological properties, J. Eur. Ceram. Soc. 41 (6) (2021 Jun 1) 3717–3730.
[16] M. Bellantone, H.D. Williams, L.L. Hench, Broad-spectrum bactericidal activity of Ag2O-doped bioactive glass, Antimicrob. Agents Chemother. 46 (6) (2002 Jun) 1940–1945.
[17] J.R. Jones, L.M. Ehrenfried, P. Saravanapavan, L.L. Hench, Controlling ion release from bioactive glass foam scaffolds with antibacterial properties, J. Mater. Sci. Mater. Med. 17 (11) (2006 Nov 1) 989–996.
[18] A.C. Marsh, N.P. Mellott, N. Pajares-Chamorro, M. Crimp, A. Wren, N.D. Hammer, et al., Fabrication and multiscale characterization of 3D silver containing bioactive glass-ceramic scaffolds, Bioact. Mater. 4 (2019 Dec 1) 215–223.
[19] M. Miola, E. Verné, C. Vitale-Brovarone, F. Baino, Antibacterial bioglass-derived scaffolds: innovative synthesis approach and characterization, Int. J. Appl. Glass Sci. 7 (2) (2016) 238–247.
[20] F.E. Ciraldo, M. Arango-Ospina, W.H. Goldmann, A.M. Beltrán, R. Detsch, A. Gruenewald, et al., Fabrication and characterization of Ag- and Ga-doped mesoporous glass-coated scaffolds based on natural marine sponges with improved mechanical properties, J. Biomed. Mater. Res. 109 (8) (2021) 1309–1327.
[21] C. Balagna, C. Vitale-Brovarone, M. Miola, E. Verné, R.A. Canuto, S. Saracino, et al., Biocompatibility and antibacterial effect of silver doped 3D-glass-ceramic scaffolds for bone grafting, J. Biomater. Appl. 25 (6) (2011 Feb 1) 595–617.
[22] P.J. Newby, R. El-Gendy, J. Kirkham, X.B. Yang, I.D. Thompson, A.R. Boccaccini, Ag-doped 45S5 Bioglass®-based bone scaffolds by molten salt ion exchange: processing and characterisation, J. Mater. Sci. Mater. Med. 22 (3) (2011 Mar 1) 557–569.
[23] C. Vitale-Brovarone, F. Baino, E. Verné, High strength bioactive glass-ceramic scaffolds for bone regeneration, J. Mater. Sci. Mater. Med. 20 (2) (2009 Feb 1) 643–653.
[24] S. Di Nunzio, E. Vernè, Process for the production of silver-containing prosthetic devices [Internet]. Turin; EP 1 819 372 B1, Available from: https://data.epo.org/publication-server/document?iDocId=3551608&iFormat=0, 2005. (Accessed 21 January 2022).
[25] M. Miola, G. Fucale, G. Maina, E. Verné, Antibacterial and bioactive composite bone cements containing surface silver-doped glass particles, Biomed. Mater. 10 (5) (2015 Oct) 055014.

[26] L.L. Hench, J. Wilson, Surface-active biomaterials, Science 226 (4675) (1984 Nov 9) 630–636.
[27] T. Kokubo, H. Takadama, How useful is SBF in predicting in vivo bone bioactivity? Biomaterials 27 (15) (2006 May 1) 2907–2915.
[28] A.L.B. Maçon, T.B. Kim, E.M. Valliant, K. Goetschius, R.K. Brow, D.E. Day, et al., A unified in vitro evaluation for apatite-forming ability of bioactive glasses and their variants, J. Mater. Sci. Mater. Med. 26 (2) (2015 Feb) 115.
[29] National Committee for Clinical Laboratory Standards, Performance Standards for Antimicrobial Disk Susceptibility Tests; Approved Standard: M2-A7, ninth ed., NCCLS, Villanova, PA, USA, 2003.
[30] N. Kavanagh, E.J. Ryan, A. Widaa, G. Sexton, J. Fennell, S. O'Rourke, et al., Staphylococcal osteomyelitis: disease progression, treatment challenges, and future directions, Clin. Microbiol. Rev. 31 (2) (2018 Feb 14) e00084, 17.
[31] F. Baino, M. Ferraris, O. Bretcanu, E. Verné, C. Vitale-Brovarone, Optimization of composition, structure and mechanical strength of bioactive 3-D glass-ceramic scaffolds for bone substitution [Internet], J. Biomater. Appl. (2011 Dec 29). Available from: https://journals.sagepub.com/doi/10.1177/0885328211429193. (Accessed 30 November 2020).
[32] C. Lara, M.J. Pascual, A. Durán, Glass-forming ability, sinterability and thermal properties in the systems RO–BaO–SiO2 (R=Mg, Zn), J. Non-Cryst. Solids 348 (2004 Nov 15) 149–155.
[33] A. Hrubý, Evaluation of glass-forming tendency by means of DTA, Czech. J. Phys. B 22 (11) (1972 Nov 1) 1187–1193.
[34] D. Bernache-assollant, Govin: structural transformations of bioactive glass 45S5 with thermal treatments, Acta Mater. 56 (2007 Jan 1). Available from: https://www.academia.edu/79060368/Govin_Structural_transformations_of_bioactive_glass_45S5_with_thermal_treatments_Acta_Materialia_56. (Accessed 29 May 2023).
[35] O. Bretcanu, X. Chatzistavrou, K. Paraskevopoulos, R. Conradt, I. Thompson, A. R. Boccaccini, Sintering and crystallisation of 45S5 Bioglass® powder, J. Eur. Ceram. Soc. 29 (16) (2009) 3299.
[36] G. Kaur, V. Kumar, F. Baino, J.C. Mauro, G. Pickrell, I. Evans, et al., Mechanical properties of bioactive glasses, ceramics, glass-ceramics and composites: state-of-the-art review and future challenges, Mater. Sci. Eng., C 104 (2019 Nov 1) 109895.
[37] K.A. Hing, Bioceramic bone graft substitutes: influence of porosity and chemistry, Int. J. Appl. Ceram. Technol. 2 (3) (2005) 184–199.
[38] S.V. Dorozhkin, M. Epple, Biological and medical significance of calcium phosphates, Angew. Chem. Int. Ed. 41 (17) (2002) 3130–3146.
[39] Ö.H. Andersson, G. Liu, K.H. Karlsson, L. Niemi, J. Miettinen, J. Juhanoja, In vivo behaviour of glasses in the SiO2-Na2O-CaO-P2O5-Al2O3-B2O3 system, J. Mater. Sci. Mater. Med. 1 (4) (1990 Nov 1) 219–227.
[40] S. Ferraris, S. Yamaguchi, N. Barbani, C. Cristallini, G. Gautier di Confiengo, J. Barberi, et al., The mechanical and chemical stability of the interfaces in bioactive materials: the substrate-bioactive surface layer and hydroxyapatite-bioactive surface layer interfaces, Mater. Sci. Eng., C 116 (2020 Nov 1) 111238.
[41] M. Cerruti, D. Greenspan, K. Powers, Effect of pH and ionic strength on the reactivity of Bioglass® 45S5, Biomaterials 26 (14) (2005 May 1) 1665–1674.
[42] M. Mačković, A. Hoppe, R. Detsch, D. Mohn, W.J. Stark, E. Spiecker, et al., Bioactive glass (type 45S5) nanoparticles: in vitro reactivity on nanoscale and biocompatibility, J. Nanoparticle Res. 14 (7) (2012 Jun 22) 966.
[43] H. Du, C.T. Williams, A.D. Ebner, J.A. Ritter, In situ FTIR spectroscopic analysis of carbonate transformations during adsorption and desorption of CO2 in K-promoted HTlc, Chem. Mater. 22 (11) (2010 Jun 8) 3519–3526.
[44] D. Groh, F. Döhler, D.S. Brauer, Bioactive glasses with improved processing. Part 1. Thermal properties, ion release and apatite formation, Acta Biomater. 10 (10) (2014 Oct) 4465–4473.
[45] X. Lu, Y. Leng, Theoretical analysis of calcium phosphate precipitation in simulated body fluid, Biomaterials 26 (10) (2005 Apr 1) 1097–1108.
[46] H. Wang, S. Zhao, X. Cui, Y. Pan, W. Huang, S. Ye, et al., Evaluation of three-dimensional silver-doped borate bioactive glass scaffolds for bone repair: biodegradability, biocompatibility, and antibacterial activity, J. Mater. Res. 30 (18) (2015 Sep 1) 2722–2735.
[47] X. Chen, J. Zhou, Y. Qian, L. Zhao, Antibacterial coatings on orthopedic implants, Mater Today Bio 19 (2023 Apr 1) 100586.
[48] A. Cochis, J. Barberi, S. Ferraris, M. Miola, L. Rimondini, E. Vernè, et al., Competitive surface colonization of antibacterial and bioactive materials doped with strontium and/or silver ions, Nanomaterials 10 (1) (2020 Jan) 120.
[49] M. Lallukka, A. Houaoui, M. Miola, S. Miettinen, J. Massera, E. Verné, In vitro cytocompatibility of antibacterial silver and copper-doped bioactive glasses [Internet], Ceram. Int. (2023 Aug 31). Available from, https://www.sciencedirect.com/science/article/pii/S0272884223025518. (Accessed 13 September 2023).